Materials Advances

ROYAL SOCIETY OF CHEMISTRY

PAPER

View Article Online
View Journal | View Issue

Cite this: *Mater. Adv.*, 2025, 6, 4364

Chitosan–acrylic acid biomaterial with an antimicrobial nature supports biomineralization and is suitable for bone tissue regeneration

Sweta Agarwal,[a] Abhishek Singh, †[a] Satish Kumar,†[b] Tejas Pravin Rokade,[b] Chandan Goswami[b] and Luna Goswami *[ac]

Received 28th November 2024,
Accepted 20th May 2025

DOI: 10.1039/d4ma01178c

rsc.li/materials-advances

Rapid increases in different pathophysiologies in mineralized tissues have imposed demands on biomaterials of natural origin to act as a surface for the regeneration of fully functional tissue. It has been reported that chitosan-based biomaterials are biocompatible, biodegradable, nontoxic, and also have antibacterial properties. However, due to the insoluble nature of chitosan, for biomaterial synthesis it needs to be dissolved in an acidic medium followed by pH neutralization. The objective of this study was to synthesize a chitosan-based biomaterial without the use of any acidic medium, followed by modification with acrylic acid in different w/v ratios. The synthesized biomaterial, *i.e.* chitosan–acrylic acid (chitosan–AA) shows uniform dispersion in water. It was further characterized for various physico-chemical properties. The obtained results indicate successful modification of the polymer, exhibiting a porous nature with a high swelling index. It shows biocompatibility against different osteogenic cell lines and supports biomineralization by osteoblasts under osteo-inductive conditions. No hemolytic effect was observed in response to the biomaterial even after prolonged exposure to blood cells. We also show that the synthesized material can be used for controlled drug release. This work demonstrates that the biomaterial can be used as a suitable surface for the adhesion and proliferation of bone cells *in vitro*.

Introduction

Advances in medical science and reductions in morbidity rates have increased the average lifespan of human beings. However, it is compromised by several lifestyle-related disorders, such as cancer, hormonal problems, changes in food habits, random and unmethodical use of therapeutic agents, and other pathophysiological problems. All of these have led to an increase in bone-related disorders, which have created new challenges for clinicians. Some frequent cases of bone-related disorders involve osteoporosis, rickets, scoliosis, Paget's disease, osteoarthritis, osteomyelitis, bone cancer and tumors.[1,2] All of these, slowly or rapidly, lead to an imbalance in skeletal integrity, disruption of vascular structures, and improper flow of nutrients, thus preventing initiation of the repair process. The primary bone repair process involves the production of certain cytokines and growth factors, followed by chondrogenesis and differentiation of bone cells into osteoblasts, osteoclasts, and osteocytes. These cells then carry out mineralization, leading to new bone formation and bone remodeling. This bone healing process is not sufficient for severe bone damage, which demands proper medical assistance and even surgical procedures. Two procedures, namely "autograft" and "allograft", are widely used, but both come with a few limitations and side effects.[3] So better and cheaper alternative options are needed to overcome these limitations.

Biomaterials can act as a scaffold for tissue engineering. There are various polymeric compounds, such as gelatin, alginate, collagen, and chitosan,[4] which are used for the synthesis of scaffold materials. Due to their diverse chemical properties, naturally occurring polysaccharides show great advantages for tissue engineering purposes. Pure forms of such polysaccharides lack stability and mechanical strength, especially under physiological conditions. To act as a suitable surface for tissue regeneration, these need to be modified with improved physicochemical and mechanical properties.[5]

Among many polymerization methods, UV-irradiation has various advantages. Due to its shorter wavelength, it holds more energy than visible light, which allows reactions to occur instantaneously with a higher rate of polymerization. Additionally, it is much safer, simpler, pollution-free and cheaper than thermal

[a] *School of Biotechnology, KIIT Deemed to be University, Patia, Bhubaneswar, Odisha, 751024, India. E-mail: lgoswami@kiitbiotech.ac.in*
[b] *School of Biological Sciences, National Institute of Science Education and Research, HBNI, Khordha, Jatni, Odisha 752050, India*
[c] *School of Chemical Engineering, KIIT Deemed to be University, Patia, Bhubaneswar, Odisha, 751024, India*
† These authors contributed equally to this work.

polymerization because it eliminates the involvement of volatile organic solvents. The method of polymerization by the UV-irradiation method involves the incorporation of the monomer on the polymer chain in the presence of photo-initiators. Photo-initiators are molecules that undergo excitation in response to light for the generation of reactive species, which are responsible for carrying out consecutive reactions. Benzophenones, alpha-hydroxy ketones, phosphine oxides, and thioxanthones are some commonly used photo-initiators. These molecules absorb photons from light to produce reactive species, and free radicals for initiation of the reaction. This method has already been used for the production of optical fibers, composites, microchips, microelectronics, coatings, adhesives, edible films, and 3D-objects.

Chitosan (CS), the second most abundant polymer after cellulose, is a naturally occurring polysaccharide composed of two arbitrarily distributed monomers, *N*-acetyl-D-glucosamine and β-(1–4)-linked D-glucosamine. It is non-toxic, biocompatible, and biodegradable, and has attracted a lot interest because of its application in the delivery of therapeutic drugs, wound dressing, and tissue engineering. The synthesis of chitosan-based biomaterial demands the initial dissolution of chitosan in acetic acid,[6,7] hydrochloric acid[8] or other acidic media. Post-synthesis and neutralization of such biomaterials with a base, for biological applications, has also been reported.

Polymers incorporating acrylic acid (as a monomer) exhibit pH sensitivity and can impart high water-absorbing capacity to the biomaterial. This pH sensitivity is imparted by the presence of the ionizable carboxylic acid functional group of the monomer. It can be polymerized with other monomers or polymers of both hydrophobic and hydrophilic nature in the presence of crosslinking agents. This ability of acrylic acid to react easily with free radicals allows the formation of copolymers with desired physicochemical properties.[9]

So far it has been found that due to lack of solubility in water, chitosan-based biomaterials need to be fabricated by dissolving them in an acidic medium,[6,7] requiring an additional step of post-synthesis neutralization for biological applications. Therefore, in this work, a simple approach was designed to synthesize a chitosan-based biomaterial by modifying the chitosan backbone with acrylic acid monomer without the use of any acidic medium to dissolve the polymer and the homogenous dispersion of chitosan–AA in water was observed. The resulting material (chitosan–AA) was further characterized for its physicochemical properties, and possibility for biological applications. To check the extent of the modification, different instrumental techniques, like UV-vis spectroscopy, FTIR and TGA, were performed. Further, to investigate whether this biomaterial is suitable to act as a surface for cell growth, the swelling index and SEM were studied which show its swelling ability and porous structure. Due to this swelling ability, chitosan–AA was utilized for a drug release assay. Additionally, from a well diffusion assay it was determined whether the inherent antimicrobial property of chitosan is retained in chitosan–AA, so that it can also be used for osteomyelitis along with bone tissue regeneration at the site. As chitosan is already known to be beneficial for bone tissue engineering, this biomaterial was used as a surface for both osteoclast and osteoblast and finally for *in vitro* biomineralization, which was further supported by Ca^{2+}-imaging. Detection of mitochondrial membrane potential and hemolysis experiments suggested no toxic effect of the biomaterial on bone cells or RBCs, respectively.

Materials and methods

Materials

Chitosan (mol wt of chitosan = 3800–20 000 Daltons, degree of deacetylation ≥75.00%), acrylic acid, sodium chloride, tryptone, yeast extract, tryptic soy broth, penicillin–streptomycin, and trypsin-EDTA (1X) were purchased from Hi-media. Sodium dodecyl sulfate, DMSO, cetyl-pyridinium chloride and MTT were purchased from MP Biomedicals (India). Benzophenone and agar-agar were purchased from Merck India. 4′-Hydroxyacetanilide was procured from TCI Chemicals Co., Ltd (India). Acetone was purchased from Sisco Research Laboratories Pvt. Ltd, (India). Milli-Q water was used for all experiments, where required.

Synthesis of chitosan–AA

Chitosan–AA 1 : 0.5, 1 : 1, 1 : 1.5 (∼weight ratio) were synthesized where sodium dodecyl sulfate (SDS) and benzophenone (initiator) were added in a 1 : 1 ratio. Briefly, 250 μL (1 : 0.5), 500 μL (1 : 1) and 750 μL (1 : 1.5) of acrylic acid (AA) were taken in different glass Petri dishes, followed by the addition of SDS and benzophenone. A fixed weight of chitosan, *i.e.* 500 mg, was added to the respective mixtures. A 1 : 1 water–ethanol solution was added gradually to obtain a thick uniform paste. The reaction mixture was exposed to UV irradiation of 365 nm for 30 min. This was followed by washing with acetone for the removal of any unreacted monomer, homopolymer, and initiator molecules. The purified sample was kept for 15–20 h in a hot-air oven at 50 °C, until dried. These variables, *i.e.* 1 : 0.5, 1 : 1, and 1 : 1.5, were used for the ∼weight ratio of chitosan to acrylic acid. The synthesis of the material is shown in a schematic diagram (Fig. 1).

Solubility of pure chitosan and chitosan–AA in water

To examine the solubility, 1% (w/v) solutions of both pure chitosan and synthesized chitosan–AA were prepared and kept on a magnetic stirrer at 80 °C and 320 rpm for 72 h.

Swelling study

This was performed by the tea bag method,[10] where a dry sample of a fixed weight was completely submerged in water at room temperature. The biomaterial was weighed at constant intervals, until it attained its maximum swelling weight. The swelling index was then calculated using the following equation:[11]

$$\text{Swelling index } (\alpha) = \frac{\text{Final wt} - \text{Initial wt}}{\text{Initial wt}} \times 100$$

The same method was performed by immersing the sample in solutions of different pH, *i.e.*, 6.2, 6.8, 7.4, and in Ringer's solution.

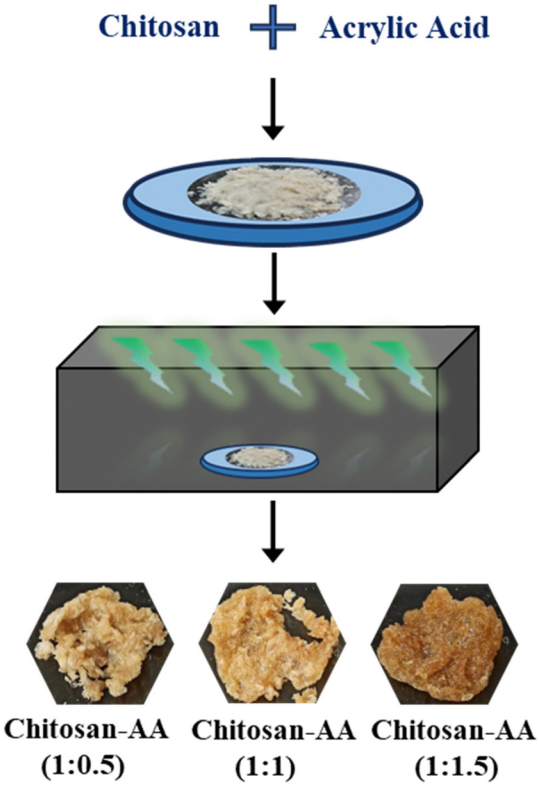

Fig. 1 Schematic diagram for the synthesis of chitosan–AA biomaterial. Schematic representation for the synthesis of the biomaterial chitosan–AA with varying ratios of chitosan to acrylic acid shown.

Spectroscopic characterization

UV-visible spectra of pure chitosan and chitosan–AA were measured in the wavelength range 200–500 nm (Agilent, Cary 100 UV-visible spectrophotometer). FTIR analysis was performed within the frequency range 400–4000 cm^{-1} (FTIR Spectrophotometer–Spectrum Two, PerkinElmer).

Thermo-gravimetric analysis (TGA)

A thermo-gravimetric analyzer was utilized to perform thermal stability analysis (TGA 4000, PerkinElmer, USA). It was carried out in the temperature range 40 °C to 700 °C in an inert environment with a constant heating rate of 20 °C min^{-1}.[12]

Microscopic structural analysis

The microscopic structure of the lyophilized sample was studied using SEM (Hitachi S3400 N) at an accelerating voltage of 15.0 kV. Sample preparation was done by freezing the swelled sample at −80 °C overnight and then lyophilizing it for 48 h. Both lateral and cross sections were cut and subjected to gold-sputtering before examination.[13] These images were also utilized to measure pore size for frequency distribution analysis.

Porosity (%) measurement

A known weight of the lyophilized sample (W_1) was immersed in a fixed volume of absolute ethanol at 25 °C. The total weight of ethanol and sample submerged in ethanol (W_2) was noted. After 24 h, the swelled sample was removed and the remaining ethanol was weighed (W_3). The porosity (%) was calculated by the volumetric displacement method, using the equation:[14]

$$\text{Porosity}\,(\%) = \frac{(W_2 - W_1 - W_3)}{(W_2 - W_3)} \times 100$$

Drug release

For drug release analysis, a fixed weight of lyophilized chitosan–AA was immersed in a solution of 4′-hydroxyacetanilide for 24 h at room temperature. The drug-loaded biomaterial was removed, wrapped in a muslin cloth and kept in the rotatory basket of a type II drug dissolution apparatus (Electrolab dissolution tester, TDT-06L).[15] 2 mL of drug dissolution solution was taken out at regular intervals and replaced by an equal volume of fresh 1X PBS (pH 7.2) solution. 1X PBS was prepared by adding NaCl, KCl, Na_2HPO_4 and KH_2PO_4 to 400 mL of distilled water. The pH was adjusted to 7.2 and the final volume was made up to 500 mL. The absorbance of the drug dissolution solution at each time point was measured at a wavelength of 249 nm (λ_{max} of 4′-hydroxyacetanilide) using a UV-visible spectrophotometer (Agilent, Cary 100 UV-visible spectrophotometer) and the drug release pattern was evaluated.

Antimicrobial efficacy

The antimicrobial properties were analyzed by a well diffusion assay. Luria–Bertani agar, and tryptic soy agar Petri plates were inoculated with Gram-negative (−ve) bacteria *Klebsiella pneumoniae* (MTCC 12 949) and Gram-positive (+ve) bacteria *Staphylococcus aureus* (ATCC 6538 and MRSA), respectively. Different concentrations of all three ratios of chitosan–AA were prepared in Milli-Q water *i.e.*, 0.6%, 1.2%, 1.8%, and added to different wells of the agar plate for each microbial strain. The Petri plates were kept at 37 °C overnight in an incubator and checked for any "zone-of-inhibition" by measuring the longest diameter of clear zone around the well.

Cell culture

RAW 264.7 cells and SaOS-2 cells (procured from NCCS Pune) were maintained in DMEM (Gibco) and McCoy's (Gibco) media enriched with 10% FBS (Gibco), and penicillin–streptomycin (Hi-Media), respectively, within an incubator maintained at 37 °C with 5% CO_2.

Biocompatibility test

To check the biocompatibility, thin films of different concentrations of the biomaterial were coated onto 12–15 mm glass coverslips and air dried. Mouse preosteoclast cells (RAW 264.7) and osteoblast cells (SaOS-2) maintained in DMEM and McCoy's media, respectively, as described earlier, were passaged using trypsin-EDTA (1X), and ~20 000 cells were seeded on the coated and uncoated coverslips and grown for 48 h in the CO_2 incubator at 37 °C. Cells were subsequently fixed using paraformaldehyde (PFA).

Nucleus and cytoskeletal staining

Cells were fixed with 4% PFA and treated with Triton-X (0.1%) to permeabilize the cell membrane. The cell cytoskeleton (actin) was subsequently stained with Alexa-488-labeled phalloidin (Invitrogen, 1 : 200) and Alexa-594-labeled phalloidin (Invitrogen, 1 : 200). Cells were further labelled with DAPI stain (1 : 2000, Invitrogen). They were then visualized under a confocal laser-scanning microscope (Olympus FV3000), and images were acquired accordingly.[16]

Detection of mitochondrial membrane potential by TMRM staining

For measurement of the mitochondrial membrane potential, RAW 264.7 and SaOS-2 cells were seeded on coverslips (25 mm) coated with or without biomaterials and allowed to grow for 48 h within the incubator set at 37 °C and CO_2 (5%). For TMRM imaging, the cells were incubated with a TMRM (tetramethylrhodamine methyl ester, perchlorate) probe (Invitrogen, 50 nM) for a duration of 0.5 h at 37 °C. Images of the cells were captured, as described for the detection of cytosolic Ca^{2+}, and TMRM intensity was plotted in GraphPad Prism.

Ca^{2+}-imaging

For the measurement of changes in Ca^{2+}-levels of osteogenic cells, SaOS-2 cells were grown for 48 h on both uncoated and biomaterial coated coverslips (25 mm) within the incubator set at 37 °C and CO_2 (5%). For Ca^{2+}-imaging, the cells were incubated with a Fluo4-AM probe (Invitrogen, 1 μM) for a duration of 0.5 h at 37 °C. Images of the cells were captured using a confocal laser-scanning microscope (Olympus FV3000). Fluo4-AM intensity and cellular parameters (area and perimeter) were plotted in GraphPad Prism for a clear comparison between the two conditions, *i.e.* biomaterial uncoated (control) and coated surface (chitosan–AA). Linear regression analysis of Fluo4-AM intensity and cellular area was also performed to determine the correlation between the two (intensity *vs*. area).[17]

Cell proliferation by MTT assay

To check the cytotoxicity, 48-well plates were coated with chitosan–AA. Approximately, 3×10^4 cells per well (RAW 264.7 and SaOS-2 separately) were seeded on both uncoated and coated surfaces and kept in a CO_2 incubator at 37 °C for 48 h. Subsequently, the medium was discarded and 200 μL (0.5 mg mL^{-1}) of MTT solution (prepared in 1X PBS) was added to the wells and kept at 37 °C for the development of formazan crystals.[12] After 4 h of incubation, DMSO was added to each well to dissolve the formazan crystals, and the optical density (O.D) was measured at 570 nm in a multimode spectral scanning reader (Thermo-Scientific Varioskan Flash).

Hemolytic compatibility

A hemocompatibility assay was performed, as described earlier[12] with slight modifications. Goat blood was collected from a slaughter house in vials pre-coated with EDTA to prevent coagulation. The collected blood samples were centrifuged thrice at 1006*g* for 10 min with washing of the pellet every single time with cold 0.9% NaCl solution. Finally, the biomaterial solution (1 mg mL^{-1} or 3 mg mL^{-1}) was gradually added to the pellet followed by incubation at 37 °C with gentle mixing for a duration of 1 h. Milli-Q water and PBS were taken as positive ('+ve') and negative ('−ve') controls, respectively. For collection of the supernatant, the samples were centrifuged at 3000 rpm for 5 min. The optical density (O.D) of the collected supernatant was measured at 540 nm with a Thermo-Scientific NANODROP ONE©, and the release of hemoglobin was determined with the equation:

$$\%\,\text{Hemolysis} = \frac{A\,(s) - A\,(-)}{A\,(+) - A\,(-)} \times 100$$

$A\,(s)$ = O.D of the sample, $A\,(-)$ = O.D of the '−ve' control, $A\,(+)$ = O.D of the '+ ve' control.

Mineralization assay *in vitro* by SaOS-2 cells

Mineralization takes place as a result of the late differentiation of osteoblastic bone cells and is a crucial phenomenon for the regeneration of bone tissue.[18] An osteo-induction medium consisting of L-ascorbic acid (100 mM), β-glycerophosphate (10 mM) and dexamethasone (10 nM) in McCoy's 5A medium was prepared for differentiation of SaOS-2 cells on both biomaterial-coated and uncoated surfaces in a 24-well plate for 10 days. Cells were then fixed using PFA (4%) followed by staining with Alizarin Red S solution (Sigma-Aldrich, India, at pH 4.2, 40 mM). Alizarin Red S selectively binds to calcium salts, developing a red color. Quantitative analysis was also performed by extracting it in 10% cetyl-pyridinium chloride solution and the absorbance (O.D.) was measured at 590 nm. Digital images of each well were also captured for representation.

Statistical study

All the graphs were created using OriginPro and GraphPad Prism 8.4.3, while all the statistical analyses were executed in GraphPad Prism 8.4.3. For comparison of two groups, an unpaired *t*-test was performed, whereas for more than two groups, one-way ANOVA was chosen, and a *p*-value of less than 0.05 was considered to be statistically significant.

Results and discussion

Synthesis of chitosan–AA

Chitin is a natural biopolymer readily available from crustacean waste and its deacetylation results in the production of chitosan. The degree of acetylation plays an immense role in its solubility.[19] Chitosan has been commonly modified using various techniques, like etherification, acylation, or alkylation, to improve its solubility.[20,21] However, in the last 30 years, acrylic-acid-modified chitosan has been synthesized in the form of microspheres,[22] polyelectrolyte complex,[23] nano-capsules,[24] interpenetrating networks,[25] nanofibers,[26] *etc.* to enhance the solubility and mechanical properties of this polymer. While most of the routes involved suspension mode synthesis *via* thermal initiation of free radical polymerization,[27–31] only a few reports

suggested synthesis *via* gamma irradiation,[32] UV irradiation[33] or photochemical initiation.[34] To date, these hydrogels/blends have been studied mostly for anticancer/gastric drug delivery applications,[35–39] wastewater treatment,[40,41] metal ions[42–44] and lipoprotein adsorption.[45] Whereas for application in bone tissue regeneration,[46] nanohydroxyapatite,[47] silica[48] or calcium carbonate[49] have been reported to be additionally incorporated in chitosan–acrylic acid blends. However, in this work chitosan–AA biomaterial was synthesized *via* UV irradiation, where chitosan was used in the solid state, eliminating the need for any acidic or organic solvent to dissolve chitosan, as required previously (Fig. 1). Hydrolysis of polymeric biomaterials is related to its bioactivity and ability to interact with the surrounding body tissue. The synthesized biomaterial was also found to be dispersed in water and was investigated for application in bone tissue regeneration.

Chitosan–AA exhibits improved solubility/dispersibility in water

Unlike pure chitosan, modified chitosan *i.e.* chitosan–AA, shows dispersion in water on continuous stirring at 80 °C. As acrylic acid is already known to impart water solubility, this change in the solubility/dispersibility pattern of chitosan might indicate the successful incorporation of acrylic acid monomer into the polymeric chitosan backbone.

Physicochemical characterization

Swelling study of all the ratios of chitosan–AA. Measurement of the swelling index of a biomaterial is a simple, safe, and inexpensive method to acquire important information about the extent of crosslinking of the polymeric chains. It also provides vital information about the structural properties that are useful for drug release and tissue engineering. It can be observed in Fig. 2a that pure chitosan shows the lowest swelling ability while it is increased to ∼2900% for chitosan–AA (1 : 0.5). The hydrophilicity further increases from chitosan–AA (1 : 0.5) to chitosan–AA (1 : 1) with the swelling index reaching ∼4000%, while it rapidly decreases thereafter for chitosan–AA (1 : 1.5). This decrease in the swelling index with increased acrylic acid concentration might be due to the incorporation of AA/PAA (polyacrylic acid) onto the polymer backbone.[50] Therefore, chitosan–AA (1 : 1) shows the highest swelling ability and was chosen for further analysis.

Swelling kinetics at different pH of PBS and Ringer's solution. The swelling ability of the biomaterial at different pH was analyzed (Fig. 2b). As chitosan is naturally soluble in an acidic medium, this chitosan-based biomaterial also shows better swelling kinetics in 1X PBS with slightly acidic pH of 6.2 and 6.8, while it is the lowest for the same at slightly alkaline pH of 7.4. Ringer's solution is a mixture of $CaCl_2$, NaCl, $NaHCO_3$, glucose, $MgSO_4 \cdot 7H_2O$, $NaH_2PO_4 \cdot H_2O$ and KCl at concentrations similar to human body fluid, which is widely used clinically to treat dehydration by restoring extracellular fluid losses and also for arthroscopic lavage. The swelling index is observed to be highest in the Ringer's solution of pH 7.3–7.4, suggesting that chitosan–AA might show better interaction with the fluid system of the human body.[51]

UV-visible spectroscopic characterization. UV-visible or electronic spectroscopy is a non-destructive analytical technique for structural interpretation. Pure chitosan shows a single peak at ∼208 nm,[52,53] acrylic acid shows a single peak at ∼205 nm,[54] while chitosan modified with acrylic acid shows two peaks: one at ∼207 nm (which is similar to pure chitosan) and the other at ∼256 nm. These absorbance peaks in chitosan–AA might suggest the successful incorporation of the acrylic acid monomer into the backbone of the chitosan polymer (Fig. 2c).

Analysis of the functional groups by Fourier transform infrared (FT-IR) spectroscopy. The infrared spectra of pure chitosan and chitosan–AA are depicted in Fig. 2d. A significant change in the spectra was observed in chitosan–AA compared to pure chitosan. The analysis of the functional group region of pure chitosan shows an intense peak at ∼3289 cm^{-1} for the stretching of the O–H and N–H groups and at ∼2869 cm^{-1} for the inter-molecular hydrogen bonds of the polysaccharide.[55] In general, the literature shows that the bands of absorption at ∼1651 (C═O), 1551 (N–H), and 1373 cm^{-1} (C–N) are due to amides I, II, and III, respectively.[56,57] In chitosan–AA, the amide I band undergoes extreme weakening, while the amide II and III bands show an increase in intensity and shift to ∼1556 and ∼1378 cm^{-1}, respectively.[52] This shift might correspond to the bending and deformation of methylene (CH_2) and methyl (CH_3) groups, respectively.[58] Sharp peaks at ∼1060, 1024 and 893 cm^{-1}, which correspond to the C–O and C–H bonds, are found to be present in both pure and modified chitosan.[55] The extreme broadening and weakening of the characteristic –OH and N–H groups of the chitosan–AA spectrum imply that it took part in the modification reaction.[59,60] The presence of such bands might indicate the incorporation of acrylic acid into the chitosan backbone.

Thermal stability analysis. Thermogravimetry is a technique to determine the thermal stability of specimens by measuring mass change with temperature. The synthesized biomaterial was analyzed for its thermal stability by TGA and its derivative DTGA thermogram, performed under inert conditions. For pure chitosan, the initial weight loss (of ∼8%) was firstly due to the elimination of the bound moisture by evaporation. This was followed by a steady weight loss (of ∼45%) initiated at 259 °C and continuing up to 400 °C, after which no weight loss is observed until 700 °C (Fig. 2e). The second stage of degradation might resemble the breakage of the polymeric chain of the neat polysaccharide.[61,62] Degradation of chitosan–AA shows a distinct reduction in the extent of degradation, as indicated by the peak values of the kinetic plot (Fig. 2f). The initial degradation (of ∼38%) was initiated at 190 °C, and continued up to 350 °C. This might be due to degradation of the acrylic acid side chains incorporated in the polymeric chain. This analysis reflects the difference in the thermograms of pure and modified chitosan.

Microstructural analysis by SEM. Morphological studies of porous samples in their native swollen state are crucial for biological application. Unlike other microscopic techniques like light microscopy and confocal microscopy, scanning electron microscopy (SEM) allows structural insights at higher resolution of sub-micron range and enhanced depth of field, without any need for chemical contrast and labels. The SEM micrograph provides details about the surface topology, nature,

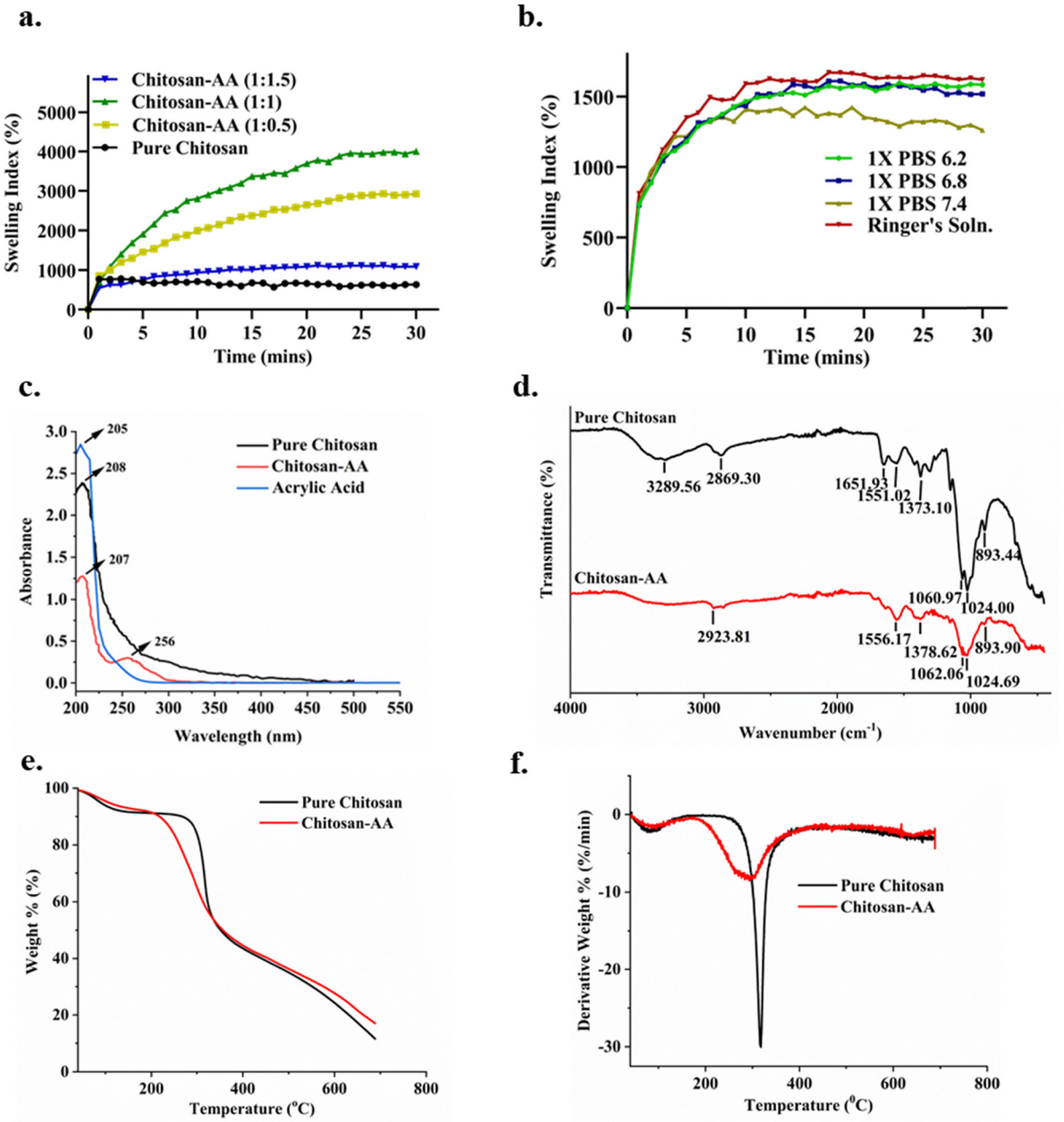

Fig. 2 Swelling index and spectroscopic characterization for pure chitosan and chitosan–AA. (a) Swelling indexes of all the ratios of chitosan–AA, where chitosan–AA (1 : 1) shows the maximum swelling ability. (b) Hydro-swelling behavior of chitosan–AA (1 : 1) in different pH solutions. Mean values of swelling index (%) from three independent experiments (n = 3). (c)–(f) Representative graphs of all the spectroscopic analysis. UV-vis spectroscopy (c) and FTIR spectra of pure chitosan and chitosan–AA indicating the successful incorporation of acrylic acid in the biomaterial chitosan–AA (d). Thermogram showing the weight retention (%) (e) and comparison of the derivative weight (%) (f) of pure chitosan and chitosan–AA.

and size of the pores present in the sample.[63] These factors are important determinants for cellular adhesion and proliferation. The lateral view (Fig. 3a) and cross-sectional (Fig. 3b) view of the lyophilized sample show that the synthesized chitosan–AA is highly porous with non-uniform pores. The frequency distribution analysis (Fig. 3c) indicates that the biomaterial exhibits pore sizes ranging from 10 μm to 100 μm, which are also interconnected. The uneven surface morphology and larger pore size satisfy the requirements for biocompatibility and application in tissue engineering purposes.[64]

Porosity (%) of chitosan–AA. Fig. 3d represents the porosity content of the biomaterial chitosan–AA. The values suggest that the biomaterial exhibits a remarkable total porosity percent of greater than 90%, which might prove its suitability for effective cell adhesion and proliferation through better uptake of nutrients.

Drug release study of chitosan–AA *in vitro*. Dissolution of a drug is a crucial parameter in the pharmaceutical industry to determine its therapeutic effectiveness and bioavailability. Drug release from a matrix involves two simultaneous

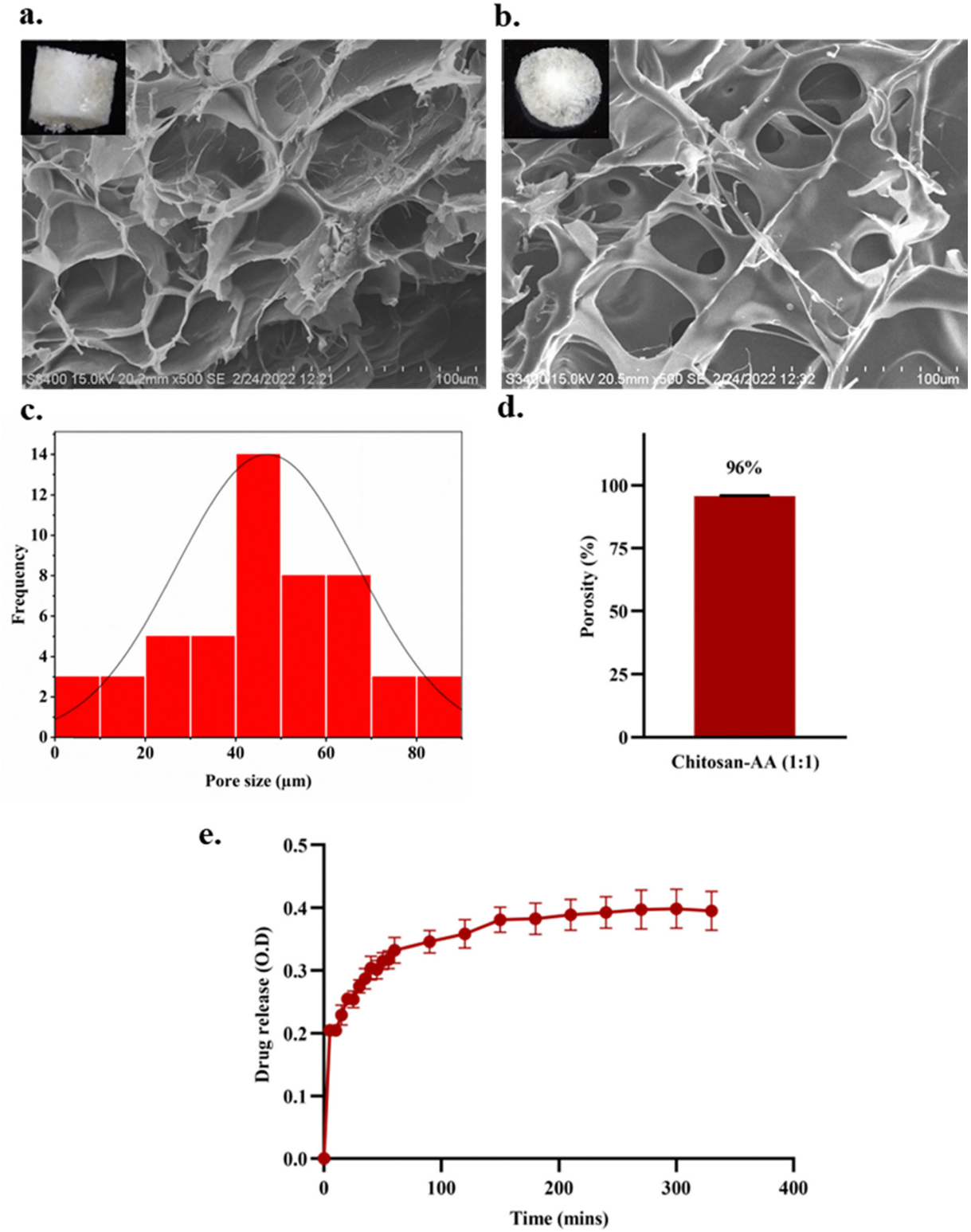

Fig. 3 Chitosan–AA has suitable pores. (a) and (b) Microstructure analysis by SEM shows the highly porous structure of chitosan–AA, as depicted in both lateral section (a) and cross section images (b). The inset images show the lyophilized sample view of the respective lateral and cross section. (c and d) Distribution pattern of pore size with pore count of 52 (calculated by SEM images using ImageJ-win64 software) (c) and porosity (%) (d). (e) Release pattern of the drug (4′-hydroxyacetanilide) from the chitosan–AA matrix in controlled pH conditions represented by mean ± SEM values of experiment performed three times.

processes of swelling with water and deswelling of the same due to the release of the drug *via* a diffusion mechanism. Fig. 3e reveals the initial release of 4′-hydroxyacetanilide within about the first 50 min followed by a sustained release

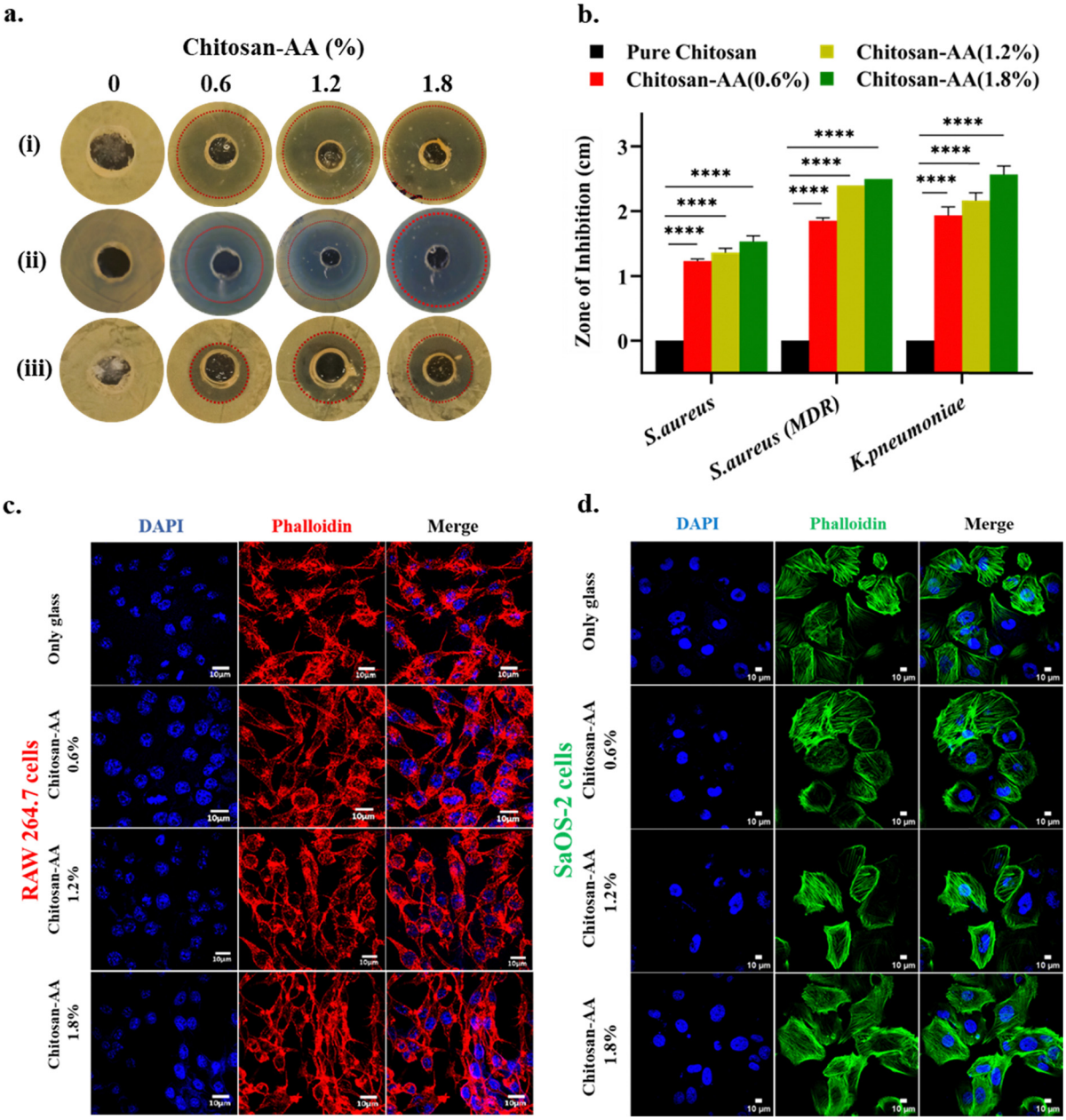

Fig. 4 Chitosan–AA has antimicrobial activities and is bio-compatible. (a) Enlarged images of the regions of Petri plates of *K. pneumoniae* (i), *S. aureus* (MDR) (ii) and *S. aureus* (iii) with clear ''zone-of-inhibition''. (b) Anti-microbial assay indicates that pure chitosan does not show any ''zone-of-inhibition'' while it increases with an increase in the concentration of chitosan–AA. The graphical representation includes mean ± SEM values of experiments, where n = 3 (i and iii) and n = 2 (ii). One-way ANOVA was performed, where **** denotes p-value < 0.0001. (c) and (d) For biocompatibility assay, mouse macrophage cells (RAW 264.7) (c) and human sarcoma osteogenic cells (SaOS-2) (d) were grown on both uncoated and biomaterial coated surface of various concentrations (*i.e.* 0.6%, 1.2% and 1.8%). Fixed cells were stained with Alexa Fluor 488-labelled (green) or Alexa Fluor 594 (red)-labelled phalloidin and DAPI (blue). Confocal images were obtained. Scale bar of 30 μm (RAW 264.7) and 50 μm (SaOS-2).

pattern for the next 4 h. This result determines that the release of drug molecules from the chitosan–AA matrix might be due to the pressure exerted by the surrounding water molecules, resulting in the replacement of drug molecules from the biomaterial matrix in dissolution media (1X PBS).

The biomaterial retains the antimicrobial property of chitosan. Infections are caused by poor antimicrobial properties of implants or biomaterial surfaces. It accounts for ∼7% of orthopedic surgery and still remains a major complication in such cases. Once biofilm formation takes place, it becomes extremely difficult to control even with high doses of antibiotics.[65] *Staphylococcus aureus*[66] and *Klebsiella pneumoniae*[67] are reported to cause bone-related infections like osteomyelitis and septic arthritis. These infections are difficult to treat because in many cases the antibiotics are unable to reach the site of infection, leading to bone loss, fractures and the need for surgery. Therefore, better

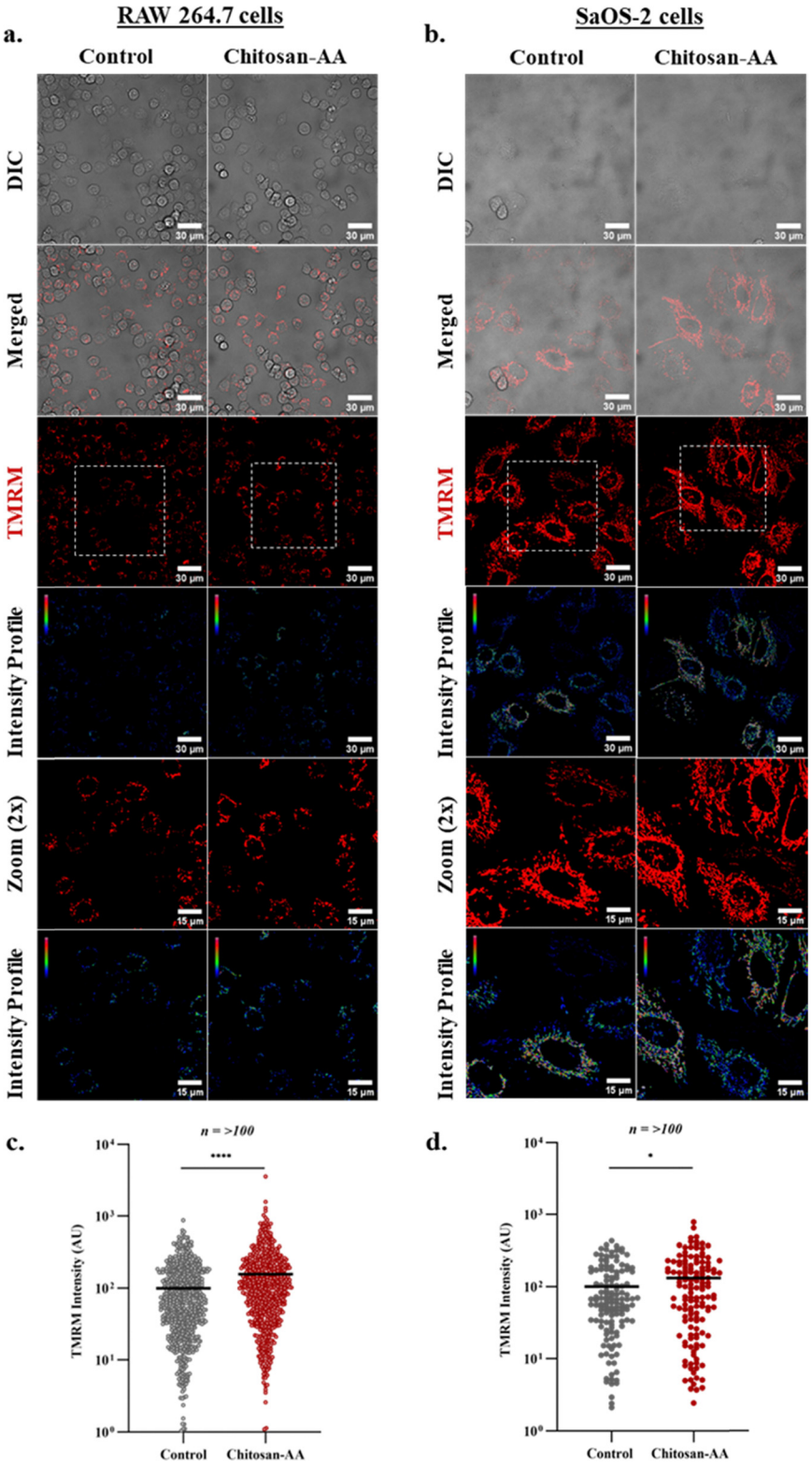

Fig. 5 Chitosan–AA improves mitochondrial membrane potential. (a) and (b) RAW 264.7 (a) and SaOS-2 (b) cells were assessed for any change in the mitochondrial membrane potential in the absence and in the presence of the biomaterial chitosan–AA. Cells were labelled with TMRM, a mitochondrial membrane potential sensor and confocal images were obtained. Scale bar of 30 μm. (c) and (d) Quantification of the images for TMRM intensity reveals a significant increase in the mitochondrial membrane potential of cells grown on the biomaterial coated surface compared to cells grown on only a glass surface for both RAW 264.7 (c) and SaOS-2 (d) cells. Statistical value of unpaired *t*-test, *p*-value: **** $<$ 0.0001 and * $<$ 0.05.

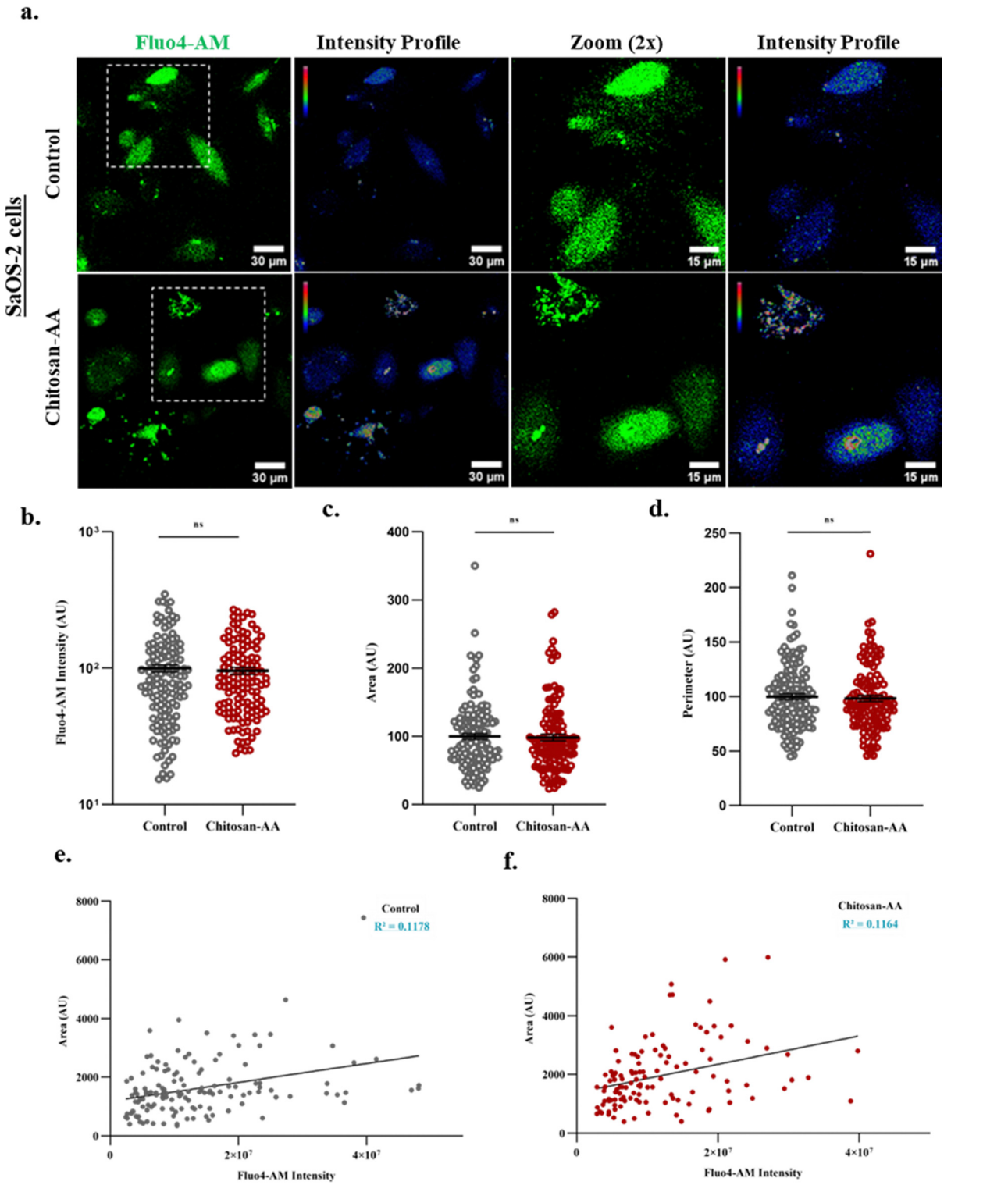

Fig. 6 Chitosan–AA does not alter the intracellular basal level Ca^{2+}. (a) Representative images of cytosolic basal-level Ca^{2+} of SaOS-2 cells grown on glass surface or on chitosan–AA surface (upper panel). Cells were probed with Fluo4-AM (30 min of incubation) followed by acquiring live cell confocal images. Respective RGB intensity profiles for Fluo4 intensity as well as for the enlarged area are shown. (b) Quantification of mean fluorescence intensity of Fluo4-AM, where $n > 100$ cells per group. (c) and (d) For quantitative analysis, images of Fluo4-AM labelled SaOS-2 cells were processed and all cellular parameters were calculated. Represented graphs depict area (c) and perimeter (d), showing no major effect of cell morphology in response to the chitosan–AA biomaterial. Unpaired *t*-test was performed by GraphPad Prism. ns (non-significant, $p > 0.05$). (e) and (f) Correlation graphs of area and Fluo4-AM intensities depict no significant difference in the R^2 values between biomaterial uncoated (control) and coated conditions. Linear regression analysis with lower R^2 values in both groups are indicative of no considerable correlation between cell morphology and cytosolic Ca^{2+}-levels.

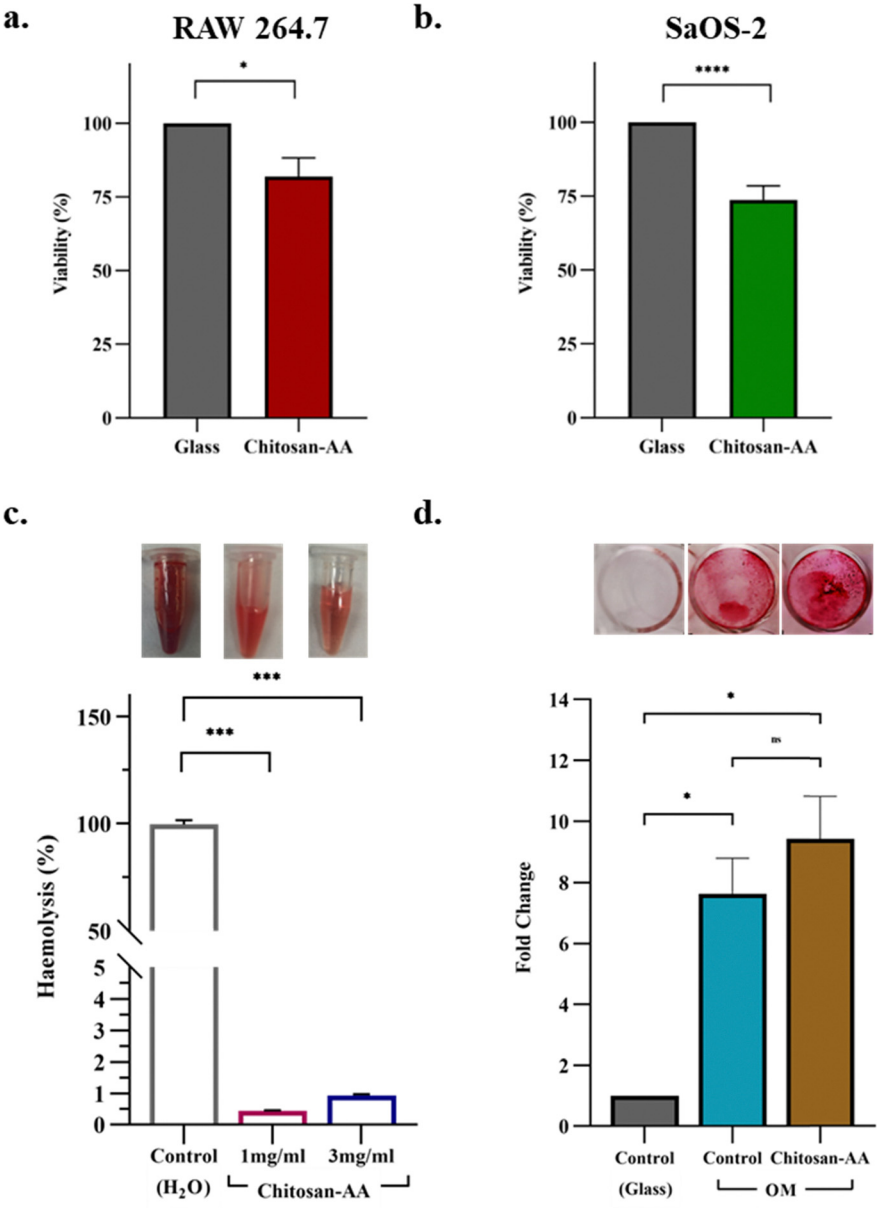

Fig. 7 Chitosan–AA is biocompatible. (a) and (b) Both RAW 264.7 (a) and SaOS-2 (b) cells attain more than 75% cell viability on chitosan–AA surface. (c) The biomaterial shows no sign of hemolysis even after prolonged exposure to blood cells. Double-distilled water is used as a positive control for hemolysis. (d) Quantitative analysis of Alizarin-stained calcium deposits by CPC extraction method. The graphical data is represented in the form of mean ± SEM. Actual images of plates with red-colored deposition of calcium complexes by SaOS-2 cells. Statistical value of unpaired *t*-test, *p*-value: **** < 0.0001, *** < 0.001, * < 0.05 and ns = non-significant.

alternatives are required to combat infection along with bone regeneration. Chitosan is known to have inherent antimicrobial properties. However, here in a well-diffusion assay, pure chitosan shows no antimicrobial effect on a relative scale (which might be due to its insolubility in water, resulting in an inability to diffuse through the agar).[68] The images of the "zone-of-inhibition" indicate that chitosan–AA can not only easily diffuse through the wells but also exhibit better antimicrobial properties against all the tested microorganisms that cause bone infection. Chitosan–AA is also equally effective against multidrug-resistant *S. aureus* (MDR). The diameter of the "zone-of-inhibition" is found to increase with increasing concentration of chitosan–AA (Fig. 4a and b).

Chitosan–AA is biocompatible with both bone-absorbing preosteoclasts and bone-forming osteoblasts. Adhesion is a crucial phenomenon in tissue engineering as it is a major prerequisite for cell growth and proliferation. Confocal images, as described in Fig. 4c and d, reveal adhesion, growth, and proliferation of RAW 264.7 (pre-osteoclast cells) and SaOS-2 (osteosarcoma) on the chitosan–AA matrix at different concentrations (w/v) (*i.e.* 0.6%, 1.2%, and 1.8%), without any morphological alterations.

Chitosan–AA exerts a positive effect on mitochondrial health. Mitochondrial health is a crucial parameter for various cellular functions. Healthy mitochondria display a potential difference between the two sides of the membrane (inside and outside of the organelle). While damaged or dead cells are incapable of maintaining this membrane potential. Therefore, to assess mitochondrial cytotoxicity, pre-osteoclast RAW 264.7 cells (Fig. 5a) and SaOS-2 (Fig. 5b) osteoblasts were labelled with a cationic, mitochondrial membrane potential selective dye, TMRM. Quantification of its fluorescent intensity from the acquired images using ImageJ, indicates a significant rise in the TMRM intensity in the presence of the biomaterial (chitosan–AA) (Fig. 5c and d), suggesting improved mitochondrial health.[17]

No visible change in Ca^{2+}-levels of osteogenic cells in response to chitosan–AA. Ca^{2+} is an essential element for various biological functions, but it has major importance in the bone mineralization process directly or indirectly. Therefore, SaOS-2 cells were grown on both surfaces, *i.e.* on coated with biomaterials as well as on an uncoated surface and were labelled with Ca^{2+}-sensitive Fluo4-AM dye and images were acquired (Fig. 6a). Quantification of Fluo4-AM intensity from the acquired images using ImageJ, indicates that the biomaterial does not exert any adverse change in the Ca^{2+}-levels of SaOS-2 cells (Fig. 6b). Additionally, the presence of chitosan–AA does not cause any significant change in the area or perimeter of the cells (Fig. 6c and d). No strong correlation was observed between intracellular Ca^{2+}-level and the area of the cells in the presence or absence of the biomaterial (Fig. 6e and f)., Additionally, no considerable difference in the R^2 value of either group (0.1178 for 'control' and 0.1164 for 'chitosan–AA') was noted. This suggests, that chitosan–AA can act as a suitable surface for cell adhesion and proliferation without drastically altering the cellular parameters.

***In vitro* cellular toxicity analysis by MTT assay.** Toxicity by MTT reduction reveals that chitosan–AA does not show any cytotoxic effect on the cells. For both pre-osteoclastic RAW 264.7 and osteoblastic SaOS-2 cells, more than 75% cell viability was attained at 48 h after seeding (Fig. 7a and b). As more than 70% viability is considered to be non-toxic, the results suggest that this biomaterial supports the growth and proliferation of bone cells.[69]

Chitosan–AA does not exert any hemolytic effect. The hemolytic assay recommended by the International Organization for Standardization (ISO) allows toxicological analysis of any biomaterial. It is one of the most important parameters for application of a biomaterial *in vivo*, to prevent any adverse reactions, like coagulation, activation, inflammation, or reduction in the numbers of each blood component. It eliminates the possibility of any degradation product of the biomaterial interacting with the components of blood, leading to detrimental effects. Chitosan–AA at concentrations of 1 mg mL^{-1} and 3 mg mL^{-1} shows $\sim$0.5% and $\sim$1% hemolysis, respectively (Fig. 7c). These values are less than the acceptable limit (5%) determined by ISO 10993-4. These results indicate no RBC lysis or release of its lysed components in response to the biomaterial, which indicates the absence or formation of any toxic degradation products from the biomaterial.

***In vitro* Ca^{2+}-deposition on chitosan–AA surface.** The growth of inorganic crystals is a crucial phenomenon for bone tissue repair and remodeling. Biomimetic mineralization on the biomaterial surface is known to augment bone regeneration by enhancing osteo-inductive and osteo-conductive activity of bone cells.[70,71] Therefore, to understand the osteogenic potential of the synthesized biomaterial, the ability to deposit an insoluble Ca^{2+}-complex was evaluated. SaOS-2 cells were seeded on both chitosan–AA-coated and uncoated surfaces in the presence of mineralization media and constantly observed for 10 days. CPC extraction and quantification of Alizarin stain calcium deposits, as shown in Fig. 7d, suggests that the chitosan–AA surface supports mineralization and shows similar fold change to that on the glass surface in the presence of osteo-inductive media. The same trend is depicted in the images of the well plate after staining with calcium-binding dye Alizarin Red S.

Conclusions

This paper entails a quick and unique approach for the fabrication of a highly porous modified chitosan-based biomaterial, without solubilizing the polymer in any low-pH solutions. Analysis indicates that the biomaterial holds excellent swelling potential, which permits favourable attachment and viability of cells, effective diffusion of nutrients, and mineralization by bone osteoblasts *in vitro*. Compared to earlier work that used an acidic medium for the dissolution of chitosan prior to biomaterial synthesis, the chitosan–AA surface developed in this work shows similar or better ability for bone cell adherence and mineralization by osteoblasts. This biomaterial can be considered as a suitable framework for bone tissue engineering due to its easy dispersion in water, antimicrobial properties, and lack of noticeable toxicity to blood and bone cells.

Author contributions

Conceptualization, investigation and methodology: Sweta Agarwal, Abhishek Singh, Chandan Goswami, Luna Goswami. Data acquisition: Sweta Agarwal, Satish Kumar, Tejas Pravin Rokade. Manuscript drafting: Sweta Agarwal, Luna Goswami. Supervision: Luna Goswami.

Data availability

Data will be made available upon reasonable request.

Conflicts of interest

There are no conflicts to declare.

Acknowledgements

Sweta Agarwal was financially supported by DST-INSPIRE Fellowship (IF180735), New Delhi, India. Authors acknowledge

infrastructure support from KIIT School of Biotechnology, KIIT, Deemed to be University. CG acknowledge NISER for central instrumental facility and intramural support from NISER/DAE. OUAT, Bhubaneswar is acknowledged for its FTIR and SEM facility. The author also thanks past and present members of the lab for their support.

References

1 A. Misaghi, A. Goldin, M. Awad and A. A. Kulidjian, *SICOT J.*, 2018, **4**, 12.
2 X. Feng and J. M. McDonald, *Annu. Rev. Pathol.: Mech. Dis.*, 2011, **6**, 121–145.
3 J. Venkatesan, B. M. Ryu, P. N. Sudha and S. K. Kim, *Int. J. Biol. Macromol.*, 2012, **50**, 393–402.
4 Y. H. Lin, K. W. Huang, S. Y. Chen, N. C. Cheng and J. Yu, *J. Mater. Chem. B*, 2017, **5**, 4614–4622.
5 P. Choudhury, S. Chawla, S. Agarwal, A. Singh, A. Nayak, A. Kumar, P. K. Maji, C. Goswami and L. Goswami, *Mater. Sci. Eng. C*, 2021, **121**, 111779.
6 Y. Huang, Y. Cai and Y. Lapitsky, *J. Mater. Chem. B*, 2015, **3**, 5957–5970.
7 M. Liu, C. Wu, Y. Jiao, S. Xiong and C. Zhou, *J. Mater. Chem. B*, 2013, **1**, 2078–2089.
8 L. S. Connell, F. Romer, M. Suárez, E. M. Valliant, Z. Zhang, P. D. Lee, M. E. Smith, J. V. Hanna and J. R. Jones, *J. Mater. Chem. B*, 2014, **2**, 668–680.
9 G. Sennakesavan, M. Mostakhdemin, L. K. Dkhar, A. Seyfoddin and S. J. Fatihhi, *Polym. Degrad. Stab.*, 2020, **180**, 109308.
10 K. Zhang, W. Feng and C. Jin, *MethodsX*, 2020, **7**, 100779.
11 S. Sanyasi, A. Kumar, C. Goswami, A. Bandyopadhyay and L. Goswami, *Carbohydr. Polym.*, 2014, **101**, 1033–1042.
12 P. Choudhury, S. Kumar, A. Singh, A. Kumar, N. Kaur, S. Sanyasi, S. Chawla, C. Goswami and L. Goswami, *Carbohydr. Polym.*, 2018, **189**, 87–98.
13 S. Kumar, R. K. Majhi, S. Sanyasi, C. Goswami and L. Goswami, *Connect. Tissue Res.*, 2018, **59**, 111–121.
14 A. Singh, S. Kumar, T. K. Acharya, C. Goswami and L. Goswami, *Mater. Today Commun.*, 2022, **31**, 103783.
15 T. K. Acharya, S. Kumar, N. Tiwari, A. Ghosh, A. Tiwari, S. Pal, R. K. Majhi, A. Kumar, R. Das, A. Singh, P. K. Maji, N. Chattopadhyay, L. Goswami and C. Goswami, *Sci. Rep.*, 2021, **11**, 3730.
16 S. Sanyasi, S. Kumar, A. Ghosh, R. K. Majhi, N. Kaur, P. Choudhury, U. P. Singh, C. Goswami and L. Goswami, *Macromol. Biosci.*, 2016, **17**, 201600268.
17 R. Chakraborty and C. Goswami, *Biochem. Biophys. Res. Commun.*, 2022, **611**, 132–139.
18 A. Singh, S. Kumar, C. Goswami and L. Goswami, *Mater. Today Chem.*, 2024, **38**, 102067.
19 I. Aranaz, A. R. Alcántara, M. C. Civera, C. Arias, B. Elorza, A. H. Caballero and N. Acosta, *Polymers*, 2021, **13**, 3256.
20 R. Pandey and G. Mathur, *Starch - Stärke*, 2024, **77**(1), 2300248.
21 A. El-Araby, W. Janati, R. Ullah, S. Ercisli and F. Errachidi, *Front. Chem.*, 2023, **11**, 1327426.
22 C. Peniche, M. Fernández, A. Gallardo, A. López-Bravo and J. San Román, *Macromol. Biosci.*, 2003, **3**, 540–545.
23 S. Y. Nam and Y. M. Lee, *J. Membr. Sci.*, 1997, **135**, 161–171.
24 S. Belbekhouche, O. Mansour and B. Carbonnier, *J. Colloid Interface Sci.*, 2018, **522**, 183–190.
25 C. Peniche, W. Arguk Elles-Monal, N. Davidenko, R. Sastre, A. Gallardo and J. S. Romah, *Biomaterials*, 1999, **20**, 1869–1878.
26 C. Y. Chen, J. W. Wang and M. H. Hon, *Macromol. Mater. Eng.*, 2006, **291**, 123–127.
27 Jayanudin, R. S. D. Lestari, D. R. Barleany, A. B. Pitaloka, M. Yulvianti, D. Prasetyo, D. V. Anggoro and A. Ruhiatna, *Polymers*, 2022, **14**, 5175.
28 C. Liu, L. Fu, T. Jiang, Y. Liang and Y. Wei, *Polymer*, 2021, **230**, 124006.
29 M. S. P. De Lima, M. S. Freire, J. L. C. Fonseca and M. R. Pereira, *Carbohydr. Res.*, 2009, **344**, 1709–1715.
30 H. Ge and S. Wang, *Carbohydr. Polym.*, 2014, **113**, 296–303.
31 Y. Hu, X. Jiang, Y. Ding, H. Ge, Y. Yuan and C. Yang, *Biomaterials*, 2002, **23**, 3193–3201.
32 S. Benamer, M. Mahlous, D. Tahtat, A. Nacer-Khodja, M. Arabi, H. Lounici and N. Mameri, *Radiat. Phys. Chem.*, 2011, **80**, 1391–1397.
33 T. T. Nge, M. Yamaguchi, N. Hori, A. Takemura and H. Ono, *J. Appl. Polym. Sci.*, 2002, **83**, 1025–1035.
34 N. Davidenko and J. San Roman, *Lat. Am. Appl. Res.*, 2007, **37**, 247–253.
35 Y. Hu, Y. Ding, D. Ding, M. Sun, L. Zhang, X. Jiang and C. Yang, *Biomacromolecules*, 2007, **8**, 1069–1076.
36 I. A. Duceac, L. Verestiuc, C. D. Dimitriu, V. Maier and S. Coseri, *Polymers*, 2020, **12**, 1–20.
37 Y. Wang, J. Wang, Z. Yuan, H. Han, T. Li, L. Li and X. Guo, *Colloids Surf., B*, 2017, **152**, 252–259.
38 J.-W. Shim and Y.-C. Nho, *J. Appl. Polym. Sci.*, 2003, **90**, 3660–3667.
39 S. Torrado, P. Prada, P. M. De La Torre and S. Torrado, *Biomaterials*, 2004, **25**, 917–923.
40 S. F. Hamza, M. M. El-Sawy, N. A. Alian and N. O. Shaker, *Egypt J. Chem.*, 2021, **64**, 6007–6015.
41 A. Shanmugapriya, A. Srividhya, R. Ramya and P. N. Sudha, *Int. J. Environ. Sci.*, 2011, **1**, 7.
42 M. Marjub, N. Rahman, N. C. Dafader, F. Sultana Tuhen, S. Sultana and F. Tasneem Ahmed, *J. Polym. Eng.*, 2019, **39**(10), 883–891.
43 M. M. Rahman, N. N. Lata, S. H. Rimu and A. H. Chisty, *Desalin. Water Treat.*, 2021, **216**, 252–262.
44 A. Sepehrianazar, *Iran. J. Chem. Chem. Eng.*, 2023, **42**(4), 1099–1110.
45 G. Fu, H. Li, H. Yu, L. Liu, Z. Yuan and B. He, *React. Funct. Polym.*, 2006, **66**, 239–246.
46 S. Saber-Samandari and S. Saber-Samandari, *Mater. Sci. Eng. C*, 2017, **75**, 721–732.
47 G. S. Sailaja, P. Ramesh, T. V. Kumary and H. K. Varma, *Acta Biomater.*, 2006, **2**, 651–657.
48 Y. J. Lin, F. C. Hsu, C. W. Chou, T. H. Wu and H. R. Lin, *J. Mater. Chem. B*, 2014, **2**, 8329–8337.

49 M. A. E. Cruz and A. P. Ramos, *Surf. Coat. Technol.*, 2016, **294**, 145–152.
50 G. Hoti, F. Caldera, C. Cecone, A. R. Pedrazzo, A. Anceschi, S. L. Appleton, Y. K. Monfared and F. Trotta, *Materials*, 2021, **14**, 1–20.
51 R. Komeri, F. G. Thankam and J. Muthu, *RSC Adv.*, 2015, **5**, 31439–31449.
52 Z. Bujňáková, E. Dutková, A. Zorkovská, M. Baláž, J. Kováč, M. Kello, J. Mojžiš, J. Briančin and P. Baláž, *J. Mater. Sci.*, 2017, **52**, 721–735.
53 H. Abdulsahib, H. T. Abdulsahib, A. H. Taobi and S. S. Hashem, *Adv. J. Sci. Res.*, 2016, **1**, 1–10.
54 L. Xue and D. J. Kieber, *J. Photochem. Photobiol., A*, 2024, **449**, 115371.
55 E. Stodolak-Zych, P. Jeleń, E. Dzierzkowska, M. Krok-Borkowicz, Ł. Zych, M. Boguń, A. Rapacz-Kmita and B. Kolesińska, *J. Mol. Struct.*, 2020, **1211**, 128061.
56 Y. Liu, X. Shen, H. Zhou, Y. Wang and L. Deng, *Appl. Surf. Sci.*, 2016, **370**, 270–278.
57 S. Mincke, T. G. Asere, I. Verheye, K. Folens, F. Vanden Bussche, L. Lapeire, K. Verbeken, P. Van Der Voort, D. A. Tessema, F. Fufa, G. Du Laing and C. V. Stevens, *Green Chem.*, 2019, **21**, 2295–2306.
58 M. F. Queiroz, K. R. T. Melo, D. A. Sabry, G. L. Sassaki and H. A. O. Rocha, *Mar. Drugs*, 2015, **13**, 141–158.
59 C. Brasselet, G. Pierre, P. Dubessay, M. Dols-Lafargue, J. Coulon, J. Maupeu, A. Vallet-Courbin, H. de Baynast, T. Doco, P. Michaud and C. Delattre, *Appl. Sci.*, 2019, **9**, 1321.
60 B. Doshi, E. Repo, J. P. Heiskanen, J. A. Sirviö and M. Sillanpää, *Carbohydr. Polym.*, 2017, **167**, 326–336.
61 M. Liu, C. Wu, Y. Jiao, S. Xiong and C. Zhou, *J. Mater. Chem. B*, 2013, **1**, 2078–2089.
62 S. Kumar and J. Koh, *Int. J. Mol. Sci.*, 2012, **13**, 6102–6116.
63 R. A. Batista, C. G. Otoni and P. J. P. Espitia, in *Materials for Biomedical Engineering: Hydrogels and Polymer-based Scaffolds*, Elsevier, 2019, pp. 61–81.
64 M. N. Collins, G. Ren, K. Young, S. Pina, R. L. Reis and J. M. Oliveira, *Adv. Funct. Mater.*, 2021, **31**, 2010609.
65 S. Kumar, R. K. Majhi, A. Singh, M. Mishra, A. Tiwari, S. Chawla, P. Guha, B. Satpati, H. Mohapatra, L. Goswami and C. Goswami, *ACS Appl. Mater. Interfaces*, 2019, **11**, 42998–43017.
66 N. Kavanagh, E. J. Ryan, A. Widaa, G. Sexton, J. Fennell, S. O'rourke, K. C. Cahill, C. J. Kearney, F. J. O'brien and S. W. Kerrigan, *Clin. Microbiol. Rev.*, 2018, **31**, e00084–17.
67 T. Kawamura, D. Ono, A. Shirai, K. Mimura, S. Iida, K. Saita, H. Oka and H. Ohno, *IDCases*, 2022, **27**, e01404.
68 A. Piegat, A. Żywicka, A. Niemczyk and A. Goszczyńska, *Polymers*, 2021, **13**, 1–13.
69 X. Liu, D. P. Rodeheaver, J. C. White, A. M. Wright, L. M. Walker, F. Zhang and S. Shannon, *Regul. Toxicol. Pharmacol.*, 2018, **97**, 24–32.
70 A. Singh, S. Kumar, T. K. Acharya, S. Kumar, S. Chawla, C. Goswami and L. Goswami, *Int. J. Biol. Macromol.*, 2024, **264**, 130605.
71 A. Singh, C. Muduli, S. P. Senanayak and L. Goswami, *Int. J. Biol. Macromol.*, 2023, **234**, 123724.